



Waste Plastic Thermal Pyrolysis Analysis by a Neural Fuzzy Model Coupled with a Genetic Algorithm

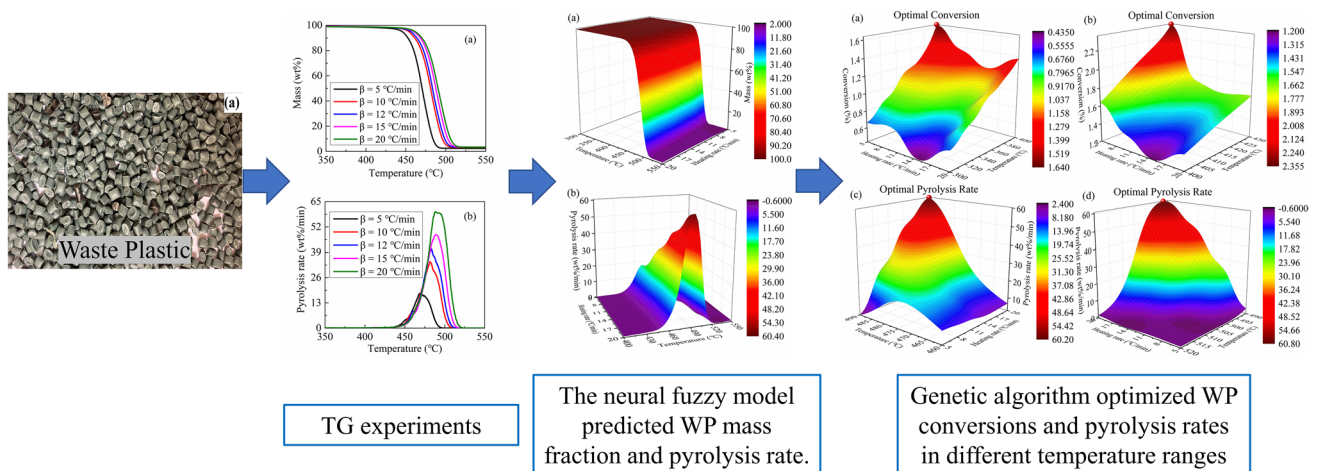
Ruming Pan¹ · João Vitor Ferreira Duque^{1,2,3} · Gérald Debenest¹

Received: 24 December 2020 / Accepted: 12 July 2021 / Published online: 23 July 2021
© The Author(s), under exclusive licence to Springer Nature B.V. 2021

Abstract

Waste plastic (WP) thermal pyrolysis is a promising method which could utilize WP to produce fuels. This study investigated this method to provide a direction for prospective industrial and commercial productions. The process temperature, the WP conversion and the pyrolysis rate are the decisive factors for industrial applications. Therefore, thermogravimetric (TG) experiments were conducted at different heating rates to obtain the experimental WP mass fraction, the WP conversion and the pyrolysis rate, which varied with the temperature and heating rate. Furthermore, a neural fuzzy model and a genetic algorithm (GA) were adopted to determine the optimal operating conditions over different temperature ranges. The neural fuzzy model-predicted WP conversion and pyrolysis rate were highly consistent with the experimental results, indicating the high accuracy of the neural fuzzy model method for this application. Moreover, the WP conversion and the pyrolysis rate optimized by the GA were 97.68% at 5.00 °C/min and 497.89 °C, and 60.66 wt%/min at 20.00 °C/min and 492.09 °C, respectively.

Graphic Abstract



Keywords Waste plastic pyrolysis · Thermogravimetric · Optimal pyrolysis rate · Neural fuzzy model · Genetic algorithm

Statement of Novelty

This study adopted a neural fuzzy model coupled with a genetic algorithm (GA) to conduct the waste plastic (WP) thermal pyrolysis analysis. The neural fuzzy model established mathematical expressions among the WP conversion and the pyrolysis rate, and the operating conditions

✉ Gérald Debenest
gerald.debenest@toulouse-inp.fr

Extended author information available on the last page of the article

(temperature and heating rate). Subsequently, GA was used to optimize the operating conditions for maximum WP conversions and pyrolysis rates in different temperature ranges.

Introduction

Waste plastic (WP) has caused large-scale environmental pollution and a health hazard to many organisms. Historically, a large amount of WP was disposed of via landfill or incineration [1]. Several methods have been proposed for treating WP in a more responsible way, namely, mechanical recycling, chemical recycling and energy recovery methods [2]. Among these methods, chemical recycling is a favorable method which can utilize the WP to produce fuels [3]. Moreover, WP thermal pyrolysis, which is performed in the absence of oxygen [4], is a most promising chemical recycling method. It can strongly reduce WP pollution while producing useful by-products such as biochar, bio-oil and syngas [5–8]. According to the literature [4], the temperature and heating rate are the determining factors in the WP pyrolysis process. Besides these, considering the economical aspect, the temperature, the conversion and the pyrolysis rate are also critical parameters for practical applications of WP pyrolysis [9–11].

Much research in thermogravimetric analysis (TG) has been conducted to try to obtain a better understanding about the WP pyrolysis process. Paraschiv et al. [12] adopted TG experimental results to determine the optimal operating parameters for hospital-based WP pyrolysis on different scales for a fixed bed reactor. Chen et al. [13] utilized TG analysis to investigate the WP co-pyrolysis process. Additionally, Navarro et al. [14] used TG analysis coupled with a distributed activation energy model to conduct a WP co-pyrolysis kinetic study. Chen et al. [15] investigating a waste phenolic fibre-reinforced plastic thermal pyrolysis process based on TG experiments with different heating rates. Singh et al. [16] adopted TG analysis to investigate the influence of the heating rate on the WP pyrolysis process. Moreover, Ippolito et al. [17] conducted TG experiments to determine the WP pyrolysis kinetic values. In conclusion, TG analysis is a promising method to investigate the WP pyrolysis process as it can provide important parameters—the WP relative weight over time and the temperature at different heating rates [18, 19]. However, TG experiments so-far could only provide the discrete mass fraction curves at disparate heating rates. This creates difficulties in determining the optimal conditions of the WP pyrolysis process. For the purpose of investigating the optimal conversion, Teng et al. [19] creatively adopted an artificial neural network (ANN) coupled with TG analysis and applied it to the *Chlorella vulgaris* pyrolysis process. In consequence, the *C. vulgaris* conversion turned out to be a continuous function of the

temperature and the heating rate. Subsequently, a mathematical algorithm was utilized to obtain the optimal operating parameters over different temperature ranges. Therefore, the application of artificial intelligence coupled with TG analysis could, ideally, determine the optimal operating conditions of the WP pyrolysis process.

The neural fuzzy model, from artificial intelligence theory, is a promising method which could establish an arithmetic expression to describe the relationship between multiple independent variables and dependent variables [20]. Sadeghizadeh et al. [21] and Ronda et al. [22] investigated the effects of multiple operating conditions on the Pb (II) adsorption efficiency using a neural fuzzy model. Calero et al. [23] adopted a neural fuzzy model to determine the optimal copper biosorption capacity under the influence of three operational parameters. Iáñez-Rodríguez et al. [24] conducted research on the optimal temperature and residence time during a crop torrefaction process using a neural fuzzy model. Nevertheless, the values of the response variables predicted by the afore-mentioned researchers using neural fuzzy models were discrete. Arithmetic expressions, established by the neural fuzzy model between the multiple operating parameters and the response variables however, are continuous. Therefore, the robustness of predicted optimal operating conditions can be improved. Hence, it is necessary to adopt a mathematical calculation method for determining the optimal operating parameters in accordance with the arithmetic expression established using a neural fuzzy model.

Regarding the global extremum calculation, the genetic algorithm (GA) is a promising method to find the optimal operating parameters based on the existing mathematical models. Javed et al. [25] utilized the GA for optimization of a hybrid energy storage system. Tuchler et al. [26] optimized the radial compressor of an automobile by evaluating the isentropic efficiency with the GA. Ascione et al. [27] conducted an optimization design of an envelope enclosure with the GA with multiple objective functional assessments. Rezaie et al. [28] adopted multiple objective functions to evaluate heat recovery in a steam generator. Subsequently, the GA was used to optimize the thermal design.

As there has been little research into the optimal WP conversion and pyrolysis rates with different temperatures and heating rates, this work aims to fully investigate the WP pyrolysis process, to provide guidance for industrial and commercial applications. This study investigated the optimal operating parameters—the temperature and the heating rate of the WP thermal pyrolysis conversions and the pyrolysis rates over different temperature ranges. Four TG experiments with different heating rates were conducted to obtain the experimental WP mass fraction during the pyrolysis process. Subsequently, the experimental WP conversion (calculated as WP conversion = 1 – WP relative weight) and the

pyrolysis rate (by derivation) were obtained. As previously discussed, the neural fuzzy model was adopted to establish arithmetic expressions to describe the relationships between the independent and dependent variables. The neural fuzzy model predicted WP mass fraction, conversion, and pyrolysis rate were highly accurate. Finally, the optimal operating conditions were determined using the GA.

Experiments and Methods

TG Experiments

The WP used for pyrolysis experiments, illustrated in Fig. 1a, was provided by Wanbei Plastic Recycling Development Base (Anhui-China). The WP is mainly composed of polyethylene (PE). In order to ensure the uniform composition of the WP, the WP was heated and melted and made into 3 mm pellets. As shown in Fig. 1b, the WP’s main functional groups are $-CH_2-$, $-CH$, $-CH_3$, and $-OH$ [29]. The TG experiments were conducted at temperatures ranging from 25 °C to 600 °C at five representative heating rates—5, 10, 12, 15 and 20 °C/min [15, 19, 30–32]. Consequently, the WP mass fraction m variation with time was obtained for different heating rates. Hence, the conversion α and the pyrolysis rate r_p were determined by the following equations.

$$\alpha = 1 - m \tag{1}$$

$$r_p = (m_{i+1} - m_i) / (t_{i+1} - t_i) \tag{2}$$

where m_i and t_i represent the i th mass fraction (wt%) and time (min) and m_{i+1} and t_{i+1} represent the $(i + 1)$ th mass fraction (wt%) and time (min).

Methods

Neural Fuzzy Model

The neural fuzzy model is inspired by the humanoid reasoning and the neural network’ structure. The neural fuzzy model was adopted for predicting the mass fractions and the WP conversion and pyrolysis rates based on the TG experimental data previously described. In the present study, there were two independent variables, i.e., the temperature and the heating rate. The certain dependent variable could be predicted by the following equation [20, 21]:

$$y_{pre} = \frac{\sum_{i=1}^n (a_i \cdot FR_i)}{\sum_{i=1}^n FR_i} \tag{3}$$

where y_{pre} , n , a_i and FR_i represent the predicted value, the number of rules, the constant of each rule and the fuzzy rule, respectively.

The fuzzy rule can be expressed with the following equation:

$$FR_i = \prod_{i=1}^m \mu_i(x_i, x_i(\Theta)) \tag{4}$$

where m , x_i , $x_i(\Theta)$ and $\mu_i(x_i(\Theta))$ represent the number of independent values, the evaluation value of the level of the independent variable, the value of independent variable and the membership function, respectively.

According to previous studies [20, 23], the Gaussian membership function $\mu_i(x_i(\Theta))$ can predict the dependent variables most accurately. Therefore, in the present study, the Gaussian membership function $\mu_i(x)$ was adopted. It can be expressed using the following equation:

$$\mu_i(x_i, x_i(\Theta)) = \exp\left(-0.5 \cdot ((x_i - x_i(\Theta)) / L)^2\right) \tag{5}$$

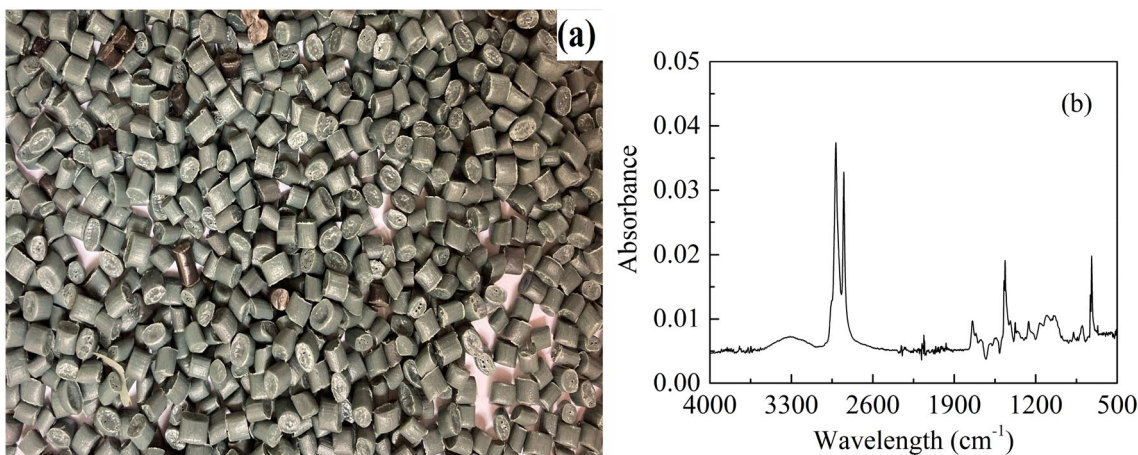


Fig. 1 WP used for pyrolysis experiments in this study: a WP pellets; b FTIR spectrum

where L represents the Gaussian distribution width.

GA

When the experimental data was processed with the neural fuzzy model, the constant of each rule a_i and the Gaussian distribution width L could be obtained. Accordingly, the GA was adopted to determine the optimal operating conditions of the WP pyrolysis process. The GA is literally developed according to evolution theory and is designed to obtain an optimal condition containing multiple chosen parameters [15, 33–37].

The WP conversion, for example, was determined by two parameters, i.e., the temperature and the heating rate. Hence, a single value for the WP conversion was considered to be an individual. It contained two “genes”, the temperature and the heating rate. A population was studied, composed of N individuals. In the first generation, these N individuals were treated as “parents”. N children were reproduced after N sets of parents underwent mutation and crossover processes. The next step was to calculate the fitness values of these N children. Children with worse fitness were replaced by children with better fitness to complete the first generation. In the next generation, these N children would be treated as the “parents” and follow the same processes as mentioned before. Therefore, the GA optimization procedure could be described using the following equations:

The mutation is expressed according to the following equation:

$$child_i^j = v_{mut} \cdot (1 - t/iter)^2 \cdot parent_i^j \quad (6)$$

where i, j, v_{mut}, t , and $iter$ represent the number of individuals, the number of genes, the probability of mutation, the number of the generation and the number of total generations, respectively.

The crossover is expressed using the following equation:

$$if r_{i,cro} < v_{cro}, child_i^j = child_n^j \quad (7)$$

where $r_{i,cro}, v_{cro}$, and n represent a random number value between 0 and 1, the probability of a crossover and the random number iteration between 1 and N , respectively.

The fitness of an individual and the highest fitness could be expressed using the following equations:

$$fitness_i = \sum_{i=1}^n (a_i \cdot FR_i) / \sum_{i=1}^n FR_i \quad (8)$$

$$fitness_{best} = \max (fitness_i) \quad (9)$$

where $fitness_i$ and $fitness_{best}$ represent the fitness of the i -th individual and the maximum value of fitness, respectively. The best child is the one with the maximum fitness value.

The replacement can be expressed with the following equation:

$$If fitness_i < 0.2 \cdot (\max (fitness_i) - \min (fitness_i)) + \min (fitness_i),$$

$$child_i^j = child_{i,best}^j \quad (10)$$

where $child_{i,best}^j$ represents the best child.

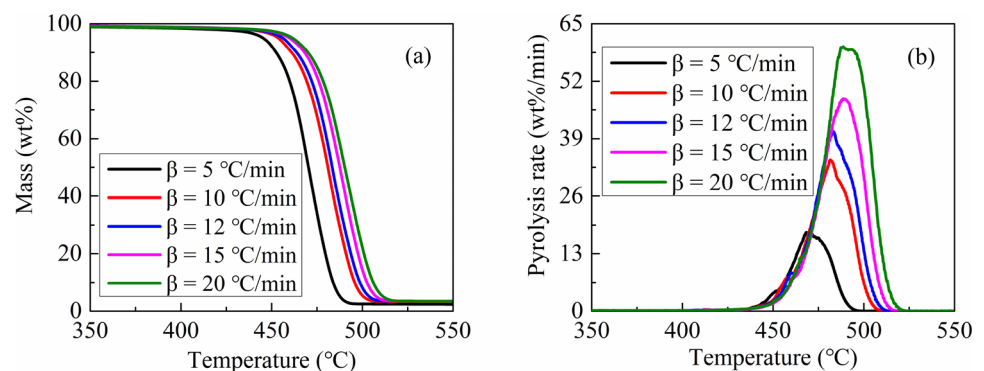
In the present study, the number of individuals N and generations $iter$ are 1000 and 1000. The probabilities of mutation v_{mut} and crossover v_{cro} are 0.2 and 0.2. Moreover, the neural fuzzy model used in the present study is from the Matlab software toolbox. The GA was also coded in Matlab.

Results and Discussion

TG Analysis

Figure 2 illustrates the experimental WP mass fractions and pyrolysis rates (which vary with the pyrolysis temperature) for heating rates of 5, 10, 12, 15 and 20 °C/min. The pyrolysis onset temperature T_o , the end pyrolysis temperature T_e and the maximum pyrolysis temperature T_m are also shown. T_o , T_e and T_m were proposed to describe the pyrolysis process more precisely [38–40]. The onset pyrolysis

Fig. 2 Experimental WP mass fractions (a) and pyrolysis rates (b) at different heating rates



temperature T_o occurs at the intersection of the tangent to the pyrolysis rate rise curve and the temperature-axis; The end pyrolysis temperature T_m occurs at the intersection of the tangent to the falling part of the pyrolysis rate curve and the temperature-axis; The maximum pyrolysis temperature T_m is the temperature coordinate value at the pyrolysis rate curve's peak. As shown in Fig. 2a, the WP mass fraction curves have the same trend regardless of the different heating rates. The WP mass fraction curve decreases slowly at the initial pyrolysis stage and the WP decomposed at a relatively high speed over a narrow temperature range. Finally, at high temperatures, the WP mass fraction curve flattened out again. Besides that, the WP mass fraction curve shifted laterally to a higher temperature when the heating rate was increased from 5 to 20 °C/min.

In terms of the pyrolysis rate, the WP had one peak at all heating rates. The single peak only represents the overall conversion rate, which does not indicate the WP is pyrolyzed in a one-step mechanism [41, 42]. The WP is decomposed into short-chain hydrocarbons via random and Beta scission reactions [43, 44]. The peak of WP pyrolysis rate curves shifted laterally to a higher temperature when the heating rate was increased from 5 to 20 °C/min, which had the same

trend as the WP mass fraction curves. Higher heating rates resulted in the thermal hysteresis from the TG instrument to WP, thereby extending the time to reach the WP's initial pyrolysis heat [45]. On the other hand, higher heating rates could accelerate the WP pyrolysis process by providing sufficient heat [45, 46]. Therefore, the maximum pyrolysis rate increased with the increasing heating rate. The WP pyrolysis rate curves were more complex compared to those for the individual plastic types [13, 14], e.g., PE, PS, PET, etc. This is because that the pyrolysis mechanism transformations are caused by the co-pyrolysis effects from the different individual plastics [13, 15, 16].

T_o , T_e , T_m and the maximum pyrolysis rates of the WP at different heating rates are listed in Table 1. The values of T_o , T_e and T_m increased with the heating rate, which is consistent with the literature results [13, 14, 17, 40, 47, 48]. While it was noticeable that the difference between T_o and T_e was quite constant, at the different heating rates, they shifted by up to 50 °C. Moreover, the WP was undergoing pyrolysis at a relatively high-speed considering the maximum pyrolysis rate values. For instance, the maximum WP pyrolysis rate could reach up to 59.82 wt%/min at a heating rate of 20 °C/min. Additionally, the pyrolysis rate also increased with the heating rate.

Table 1 T_o , T_e , T_m and the WP maximum pyrolysis rates for different heating rates

Heating rate (°C/min)	T_o (°C)	T_e (°C)	T_m (°C)	Maximum pyrolysis rate (wt%/min)
5	442.54	485.14	468.05	17.60
10	451.57	498.64	478.49	34.19
12	454.58	502.39	480.72	40.65
15	459.05	506.59	486.78	48.02
20	460.15	510.19	487.77	59.82

Neural Fuzzy Model Predicted Results

In Fig. 3, the WP mass fraction and the pyrolysis rate were determined as functions of the temperature and the heating rate using the neural fuzzy model. Experimental data obtained for different heating rates—5, 10, 15 to 20 °C/min was used. In order to reduce the calculation time, the data set used by the neural fuzzy model to predict the WP mass fraction and pyrolysis rate was sampled to be one fifth the size of the experimental data. The experimental data was

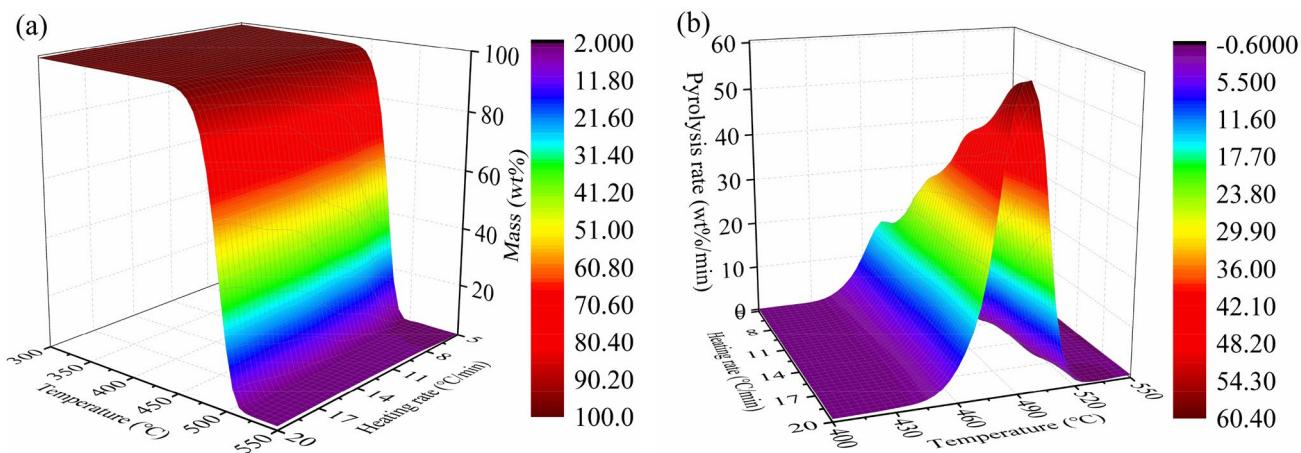


Fig. 3 The neural fuzzy model predicted WP mass fraction (a) and pyrolysis rate (b)

chosen with equal time intervals. As depicted in Fig. 3a, the WP mass fraction predicted by the neural fuzzy model followed the same trend as the experimental data. The slope of the predicted WP mass fraction surface was small in the temperature range of 300–400 °C. Subsequently, the slope became very steep at the temperature range of 400–500 °C. However, the predicted WP mass fraction surface became flat again after a pyrolysis temperature of 500 °C. Regarding the effect of the heating rate on the WP mass fraction during the pyrolysis process, the surface becomes bumpy when the heating rate is close to 10 °C/min. In addition, the WP mass fraction decreased faster at a higher heating rate, which was consistent with the results obtained experimentally for the WP mass fraction, as depicted in Fig. 2.

As for the predicted pyrolysis rate of the WP, it was noteworthy that the peak value increased with the heating rate as illustrated in Fig. 3b. This was in good agreement with the experimental WP pyrolysis rate as shown in Fig. 2b. At first, the predicted pyrolysis rate increased with temperature, then at higher temperatures it decreased. The temperature of the maximum pyrolysis rate became higher when the heating rate increased.

The Accuracy of the Neural Fuzzy Model

In Figs. 4a–d the WP mass fraction and pyrolysis rate obtained experimentally were compared with the neural fuzzy model predictions at different heating rates of 5, 10, 15 and 20 °C/min, respectively. Additionally, we calculated the R-squared values between the experimental and the predicted WP mass fraction and pyrolysis rates to determine the accuracy of the neural fuzzy model. The R-squared values of the WP mass fraction and the pyrolysis rates at heating rates of 5, 10, 15 and 20 °C/min are depicted in Figs. 4e, f, respectively. In Figs. 4a–d, the predicted WP mass fraction and the pyrolysis rate are in good agreement with the experimental values regardless of the temperature and heating rate. The coincidence degrees between the experimental and the predicted WP mass fraction were very high at all heating rates. As demonstrated in Fig. 4e, the R-squared values of the WP mass fraction were 0.99999 at heating rates of 5, 10, 15 and 20 °C/min. The R-squared values were close to 1 for every heating rate which indicated that the neural fuzzy model predicted values were highly accurate [45].

As for the WP pyrolysis rate, the neural fuzzy model predicted results also coincided with the experimental results to a great extent. For a heating rate of 5 °C/min, as illustrated in Fig. 4a, the predicted and the experimental WP pyrolysis rates had the same trend. The maximum experimental WP pyrolysis rate was 17.18 wt%/min at 467.5 °C. The maximum predicted WP pyrolysis rate was 17.73 wt%/min at 472.5 °C. The agreement between the experimental and the predicted maximum pyrolysis rates was within 3.2%.

For the heating rate of 10 °C/min, as depicted in Fig. 4b, the maximum experimental and the predicted WP pyrolysis rates were 33.80 wt%/min at 482.5 °C, and 32.59 wt%/min at 482.5 °C, respectively. The difference between the experimental and the predicted maximum pyrolysis rates was around 3.6%. As shown in Fig. 4c, the peak values of the experimental and the predicted WP pyrolysis rate curves at 15 °C/min were 47.81 wt%/min at 490.0 °C, and 47.59 wt%/min at 487.5 °C, respectively. The error of the peak values between the experimental and the predicted maximum pyrolysis rates was 0.46%. For a heating rate of 20 °C/min, as illustrated in Fig. 4d, the maximum experimental and the predicted WP pyrolysis rates were 59.51 wt%/min at 489.3 °C, and 60.63 wt%/min at 491.7 °C, respectively. The difference between the experimental and the predicted maximum pyrolysis rates was 1.9% at a rate of 20 °C/min. As described in Fig. 4f, the R-squared values of the WP pyrolysis rate were 0.99674, 0.99697, 0.99923 and 0.99934 at heating rates of 5, 10, 15 and 20 °C/min, respectively. In conclusion, the neural fuzzy model allowed for a high accuracy in predicting the WP mass fractions and pyrolysis rates.

GA Optimization

GA is a promising optimization method to determine the multiple operating parameters needed to obtain the optimal objective results. In this study, GA is used to calculate the optimal WP conversions and pyrolysis rates in different pyrolysis temperature ranges, based on neural fuzzy model predicted data. From the experimental WP mass fractions described in Fig. 2, it could be concluded that the WP pyrolysis process started at about 300 °C and finished at around 550 °C. Simultaneously, the WP pyrolysis process proceeded relatively slowly before 400 °C. Hence, according to [19], 6 temperature ranges were chosen to investigate the optimal WP conversions: 300–400 °C, 400–430 °C, 430–460 °C, 460–490 °C, 490–520 °C, and 520–550 °C, in this sequence. The optimal WP conversions in different temperature ranges calculated using GA are shown in Figs. 5a–f. As depicted in Fig. 5a, generally a larger WP conversion was obtained for a higher pyrolysis temperature and lower heating rate. For instance, the WP conversion increased from 0.66% to 1.37% when the pyrolysis temperature increased from 300 °C to 400 °C at 20 °C/min. Furthermore, the WP conversions were enhanced from 1.37% to 1.64% when the heating rate decreased from 20 to 5 °C/min. Additionally, a hollow appeared at around 15 °C/min on the WP conversion surface, as seen in Fig. 5a. The same situation occurred for the temperature range of 400–430 °C shown in Fig. 5b. Subsequently, the optimal WP conversion determined using the GA was 1.64% at 5.00 °C/min and 400 °C. The optimal WP conversions were 2.35% at 5.00 °C/min and 430.00 °C, 20.31% at 5.00 °C/min and 460.00 °C, 96.24% at 5.00 °C/

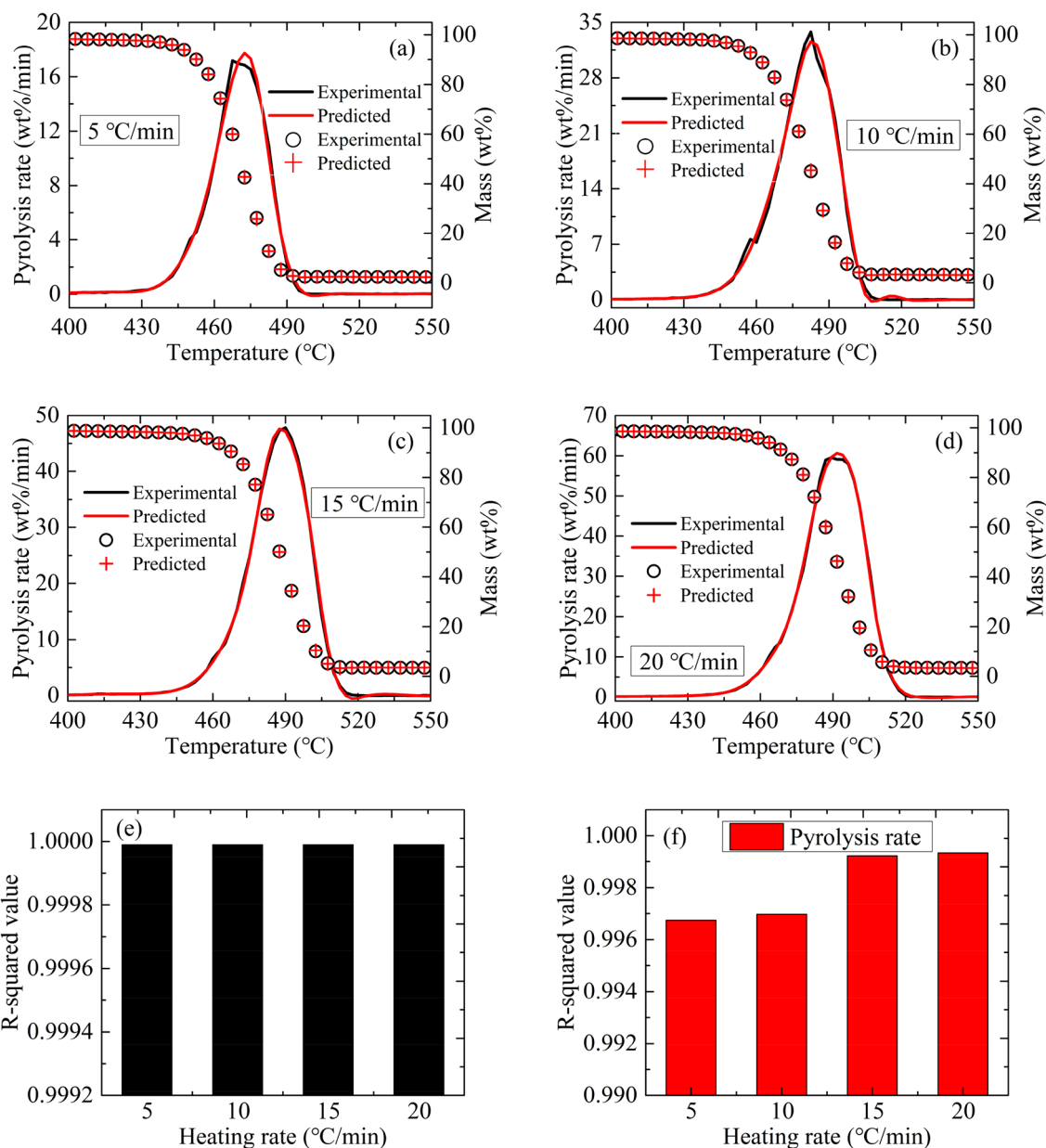


Fig. 4 Comparisons of the experimental WP mass fraction and the pyrolysis rate with the neural fuzzy model predicted values: **a** At 5 °C/min; **b** At 10 °C/min; **c** At 15 °C/min; **d** At 20 °C/min; **e** R-squared values of the WP mass fraction; **f** R-squared values of the WP pyrolysis rate

min and 490.00 °C, 97.68% at 5.00 °C/min and 497.89 °C, and 97.63% at 5.00 °C/min and 550 °C in the temperature ranges of 400–430 °C, 430–460 °C, 460–490 °C, 490–520 °C, and 520–550 °C, respectively. It is noteworthy that the predicted WP conversion slightly lowered from 97.68% to 97.63% when the temperature increased from 497.89 °C to 550 °C, which contradicted the other results of the experiment. However, the difference value was just – 0.05%, which is almost negligible.

Figures 5g, h depict the experimental and predicted optimal WP conversions for temperature ranges of 300–400 °C,

400–430 °C, 430–460 °C, 460–490 °C, 490–520 °C and 520–550 °C. These temperature intervals are denoted as 1 to 6, respectively in Figs. 5g, h. As shown in Fig. 5g, the experimental WP conversions were 1.59%, 2.43%, 20.11%, 96.39%, 97.51% and 97.63% at a heating rate of 5.00 °C/min, and at temperatures of 400.00 °C, 430.00 °C, 460.00 °C, 490.00 °C, 497.89 °C and 550.00 °C, respectively. Moreover, as demonstrated in Fig. 5h, the relative errors between the experimental and the predicted optimal WP conversions for different temperature ranges were 3.18%, – 3.25%, 0.96%, – 0.16%, 0.17% and 0.00%. The absolute values

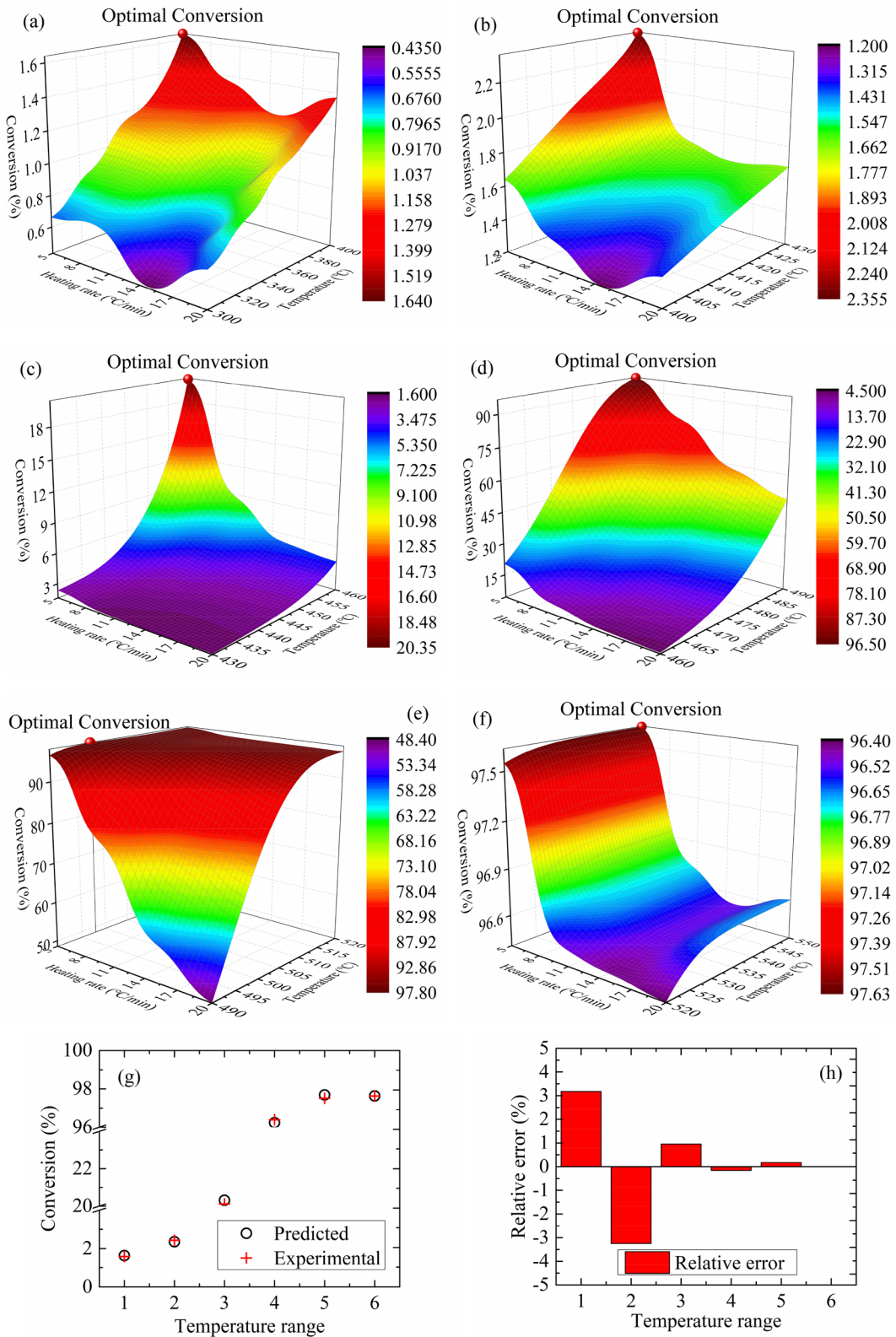


Fig. 5 Optimal WP conversions in different temperature ranges calculated using GA: **a** 300–400 °C; **b** 400–430 °C; **c** 430–460 °C; **d** 460–490 °C; **e** 490–520 °C; **f** 520–550 °C; **g** Experimental and pre-

dicted optimal conversions; **h** Relative errors between experimental and predicted optimal conversions

of the relative error were less than 3.50%. Moreover, the deviation percentage $Dev\%$ between the experimental and predicted WP conversions was 0.13, which satisfied the fitting acceptability $Dev\% < 4$, according to [14, 49]. This also indicated a satisfactory accuracy for the WP conversions predicted by the neural fuzzy model.

Figure 6 describes the optimal WP pyrolysis rates for the different temperature ranges calculated using the GA. Because of the low pyrolysis rate before 400 °C and after 550 °C, 5 temperature ranges were used to investigate the WP optimal pyrolysis rates, i.e., 400–430 °C, 430–460 °C, 460–490 °C, 490–520 °C, and 520–550 °C, in this sequence [19]. The GA determined optimal WP pyrolysis rates in different temperature ranges are depicted in Figs. 6a–e. As shown in Fig. 6a, the WP pyrolysis rate decreased with a heating rate of around 5–10 °C/min, while it increased with a heating rate of around 10–20 °C/min in a temperature range of around 400–405 °C. Moreover, in the temperature range of 405–425 °C, the WP pyrolysis rate decreased with a heating rate from around 5–10 °C/min, increased with a heating rate of around 10–15 °C/min, and decreased again with a heating rate of around 15–20 °C/min. Consequently, the optimal WP pyrolysis rate determined by the GA was 0.39 wt%/min at 20.00 °C/min and 430.00 °C in the temperature range of 400–430 °C. Furthermore, as depicted in 6b–e, the GA optimized WP pyrolysis rates were 9.78 wt%/min at 5.00 °C/min and 460.00 °C, 60.07 wt%/min at 20.00 °C/min and 490.00 °C, 60.66 wt%/min at 20.00 °C/min and 492.09 °C, and 0.84 wt%/min at 20.00 °C/min and 520.00 °C in the temperature ranges of 430–460 °C, 460–490 °C, 490–520 °C, and 520–550 °C, respectively. In conclusion, the optimal heating rate is 20 °C/min in the lower temperature range (400–430 °C) and the higher temperature range (460–550 °C), while the optimal heating rate is 5 °C/min in the medium temperature range (430–460 °C). Higher heating rates could accelerate the WP's mass loss, thereby increasing the pyrolysis rate [4]. However, higher heating rates can also cause thermal hysteresis, which is not conducive to the thermal decomposition of WP [3]. The thermal hysteresis might have a stronger influence on the WP's pyrolysis than the acceleration of WP's mass loss in the medium temperature range, thus the lowest heating rate was most conducive to the reaction rate of WP's pyrolysis. Moreover, the maximum WP pyrolysis rate was obtained at 492.09 °C and 20.00 °C/min.

Figures 6f, g illustrate the experimental and the GA optimized WP pyrolysis rates in the temperature ranges of 400–430 °C, 430–460 °C, 460–490 °C, 490–520 °C, and 520–550 °C, denoted 1 to 5 respectively in Figs. 6f, g. As demonstrated in Fig. 6f, the experimental WP pyrolysis rates were 0.39 wt%/min, 9.68 wt%/min, 59.25 wt%/min, 59.14 wt%/min, and 0.53 wt%/min in the temperature ranges of 400–430 °C, 430–460 °C, 460–490 °C, 490–520 °C, and

520–550 °C, respectively. Furthermore, as described in Fig. 6g, the relative errors between the experimental and the predicted optimal WP pyrolysis rates in the different temperature ranges were 0.57%, 1.04%, 1.39%, 2.57%, and 57.63%. Except for the temperature range of 520–550 °C, the absolute values of relative error between the experimental and the predicted optimal pyrolysis rates were less than 2.6%. The temperature range of 520–550 °C was approaching the end of the WP pyrolysis [43], in which the highest pyrolysis rate was merely 0.53 wt%/min. Although the relative error was high, the difference between predicted and the experimental optimal pyrolysis rates was only 0.31 wt%/min in the temperature range of 520–550 °C. Besides, the deviation percentage $Dev\%$ between the experimental and predicted WP pyrolysis rates was 1.33, which showed the high accuracy of the neural fuzzy model predicted results [14, 49].

Applicability of the Neural Fuzzy Model

For the purpose of certifying the applicability of the neural fuzzy model, one fifth of the experimental data for the WP conversion and the pyrolysis rate, different from that used for predicting by the neural fuzzy model, was sampled at equal interval for comparison with the neural fuzzy model predicted results. Figures 7a–e illustrate the comparison between the experimental and predicted WP mass fractions and pyrolysis rates at heating rates of 5–20 °C/min, respectively. Overall, the predicted WP mass fraction and the pyrolysis rate were consistent with the experimental data. Moreover, in order to determine the reliability of the neural fuzzy model predicted data, the R-squared values of the WP conversion and the pyrolysis rate were calculated, as depicted in Figs. 7f, g. It was noteworthy that the accuracy of the neural fuzzy model prediction of the WP mass fraction was lower at 12 °C/min compared to the predicted data at heating rates of 5, 10, 15 and 20 °C/min. As shown in Fig. 7e, the R-squared value of the WP conversion at 12 °C/min was 0.99996, while the R-squared values of the WP conversion were all 0.99999 at heating rates of 5, 10, 15 and 20 °C/min, respectively. The R-squared values of the WP mass fraction were all close to 1 at heating rates of 5–20 °C/min, exhibiting a high accuracy for the neural fuzzy model predicted values.

In terms of the WP pyrolysis rate, the neural fuzzy model predicted results were in good agreement with the experimental data. As described in Fig. 7a, the predicted and experimental WP pyrolysis rate curves almost coincided with each other at 5 °C/min. Moreover, the predicted and the experimental maximum pyrolysis rates were 17.66 wt%/min at 473.8 °C, and 17.73 wt%/min at 468.8 °C, respectively. The relative error between the predicted and the experimental maximum pyrolysis rates was around 0.39%.

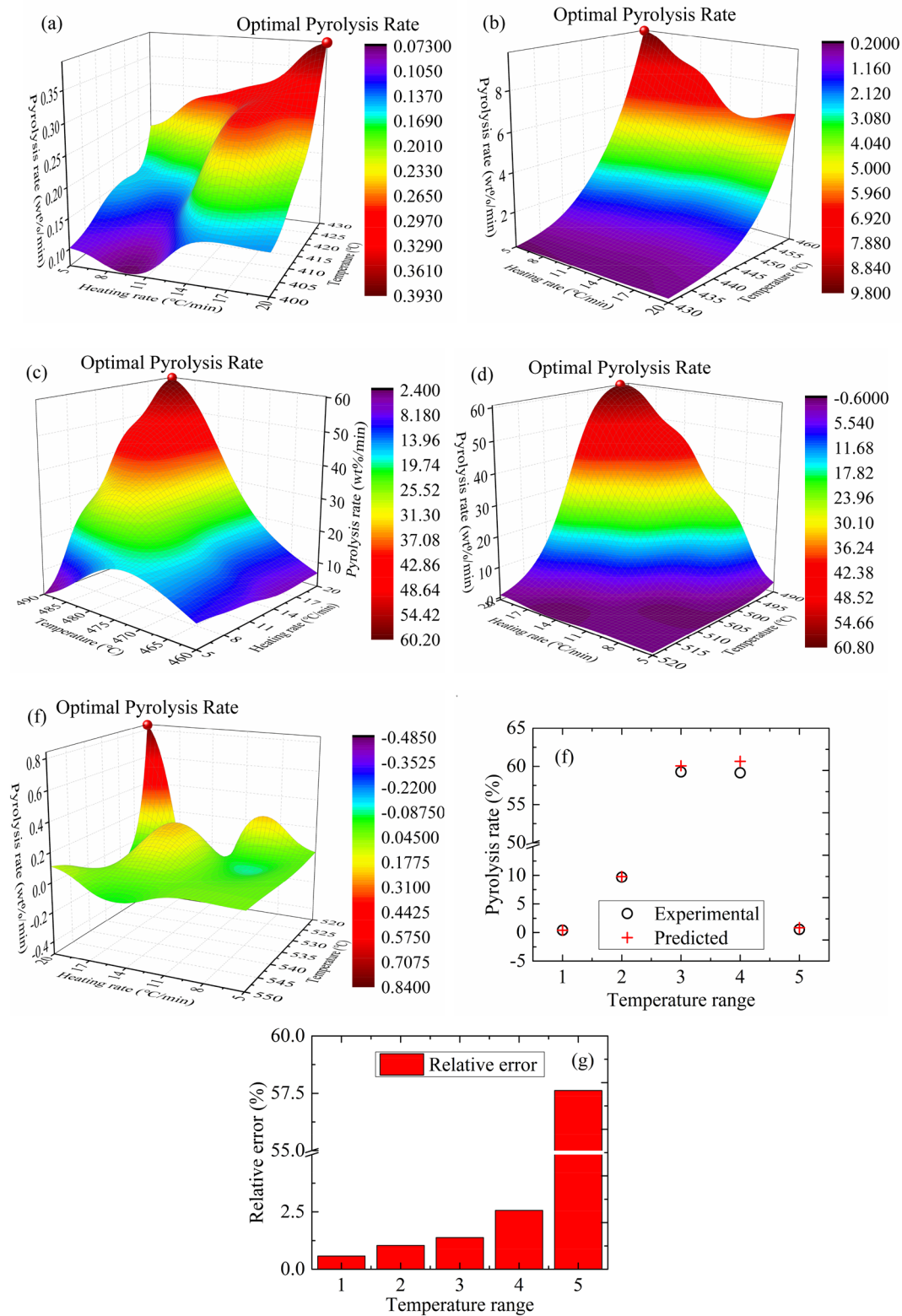


Fig. 6 Optimal WP pyrolysis rates in different temperature ranges calculated using GA: **a** 400–430 °C; **b** 430–460 °C; **c** 460–490 °C; **d** 490–520 °C; **e** 520–550 °C; **f** Experimental and predicted optimal

pyrolysis rates; **g** Relative errors between experimental and predicted optimal pyrolysis rates

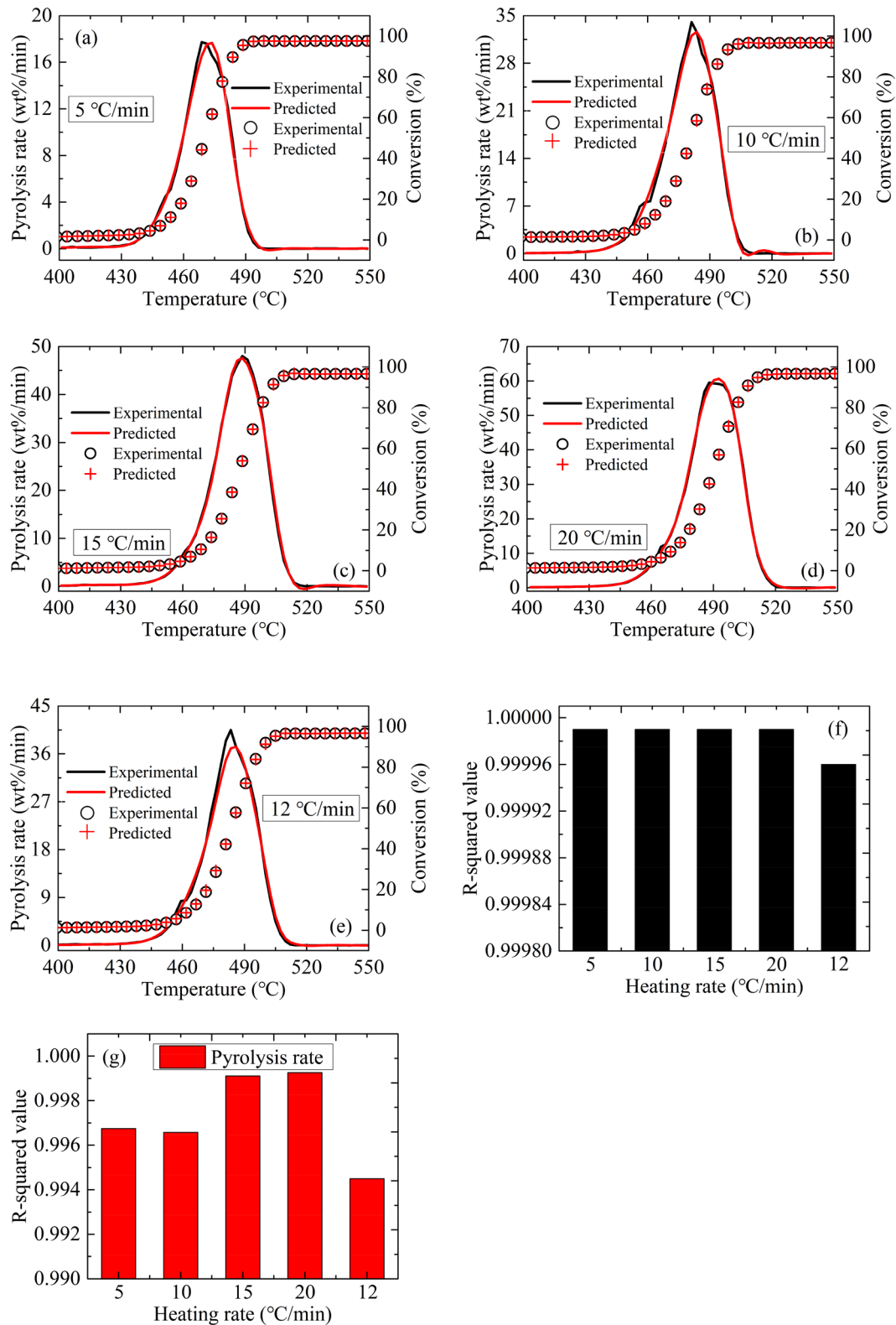


Fig. 7 Applicability of the neural fuzzy model: **a** At 5 °C/min; **b** At 10 °C/min; **c** At 15 °C/min; **d** At 20 °C/min; **e** At 12 °C/min; **f** R-squared values of the WP mass fraction; **g** R-squared values of the WP pyrolysis rate

As depicted in Fig. 7b, the predicted and the experimental maximum pyrolysis rates at 10 °C/min were 32.62 wt%/min at 483.7 °C, and 34.04 wt%/min at 481.2 °C, respectively. The agreement between the predicted and the experimental maximum pyrolysis rates was within 4.18%. As illustrated in Fig. 7c, the peak values of the predicted and experimental WP pyrolysis rate curves were 47.61 wt%/min and 48.02 wt%/min at 488.8 °C, respectively. The relative error of the peak values between the predicted and the experimental maximum pyrolysis rates was 0.84%. As shown in Fig. 7d, the predicted and the experimental maximum pyrolysis at 20 °C/min were 60.61 wt%/min at 492.7 °C, and 59.52 wt%/min at 488.0 °C, respectively. The relative error between the experimental and predicted maximum pyrolysis rates was around – 1.84%. Additionally, as demonstrated in Fig. 7f, the R-squared values of the WP pyrolysis rates were 0.99675, 0.99658, 0.99911 and 0.99926 at heating rates of 5, 10, 15 and 20 °C/min, respectively. Moreover, the R-squared value of the WP pyrolysis rate was 0.99449 at 12 °C/min, which indicated that the neural fuzzy model predicted values were highly precise.

Conclusion

This study investigated the WP thermal pyrolysis process to provide guidance for prospective industrial and commercial applications. The temperature, the conversion and the pyrolysis rate are the determining factors for industrial applications. Therefore, TG experiments were conducted at different heating rates of 5, 10, 12, 15 and 20 °C/min to obtain the WP mass fraction, the conversion and the pyrolysis rate, which varied with the temperature and heating rate. A neural fuzzy model was adopted to predict the WP conversion and the pyrolysis rate based on the experimental TG data. According to the experimental results, the WP conversion and the pyrolysis rate were investigated for the temperature ranges of 300–550 °C and 400–550 °C, respectively. Furthermore, the GA was adopted to determine the optimal operating conditions in the different temperature ranges. The neural fuzzy model was validated using the comparison of the experimental and predicted results. The accuracy of neural fuzzy model predicted results was investigated by determining the R-squared values of the mass fraction (~ 1) and the pyrolysis rate (> 0.994) compared with the available experimental observations. Subsequently, the GA optimized WP conversion and the pyrolysis rate were 97.68% at 5.00 °C/min and 497.89 °C, and 60.66 wt%/min at 20.00 °C/min and 492.09 °C, respectively. Additionally, the neural fuzzy model predicted results were consistent with the supplementary experimental data, which certified the applicability of the neural fuzzy model. The hybrid algorithm of the neural fuzzy model coupled with GA could be used to model

and analyze the co-pyrolysis behavior of WP and other materials (biomass, waste paper, etc.).

Acknowledgements This work was supported by the China Scholarship Council (CSC) program (No. 201906120036).

Data Availability Data available on request from the authors.

Declarations

Conflict of interest The authors declare no competing financial interest.

References

- Rabl, A., Spadaro, J.V., Zoughaib, A.: Environmental impacts and costs of solid waste: a comparison of landfill and incineration. *Waste Manage. Res.* **26**(2), 147–162 (2008). <https://doi.org/10.1177/0734242X07080755>
- Al-Salem, S.M., Lettieri, P., Baeyens, J.: Recycling and recovery routes of plastic solid waste (PSW): a review. *Waste Manage.* **29**(10), 2625–2643 (2009). <https://doi.org/10.1016/j.wasman.2009.06.004>
- Al-Salem, S.M., Antelava, A., Constantinou, A., Manos, G., Dutta, A.: A review on thermal and catalytic pyrolysis of plastic solid waste (PSW). *J. Environ. Manage.* **197**, 177–198 (2017). <https://doi.org/10.1016/j.jenvman.2017.03.084>
- Sharuddin, S.D.A., Abnisa, F., Daud, W.M.A.W., Aroua, M.K.: A review on pyrolysis of plastic wastes. *Energy Convers. Manage.* **115**, 308–326 (2016). <https://doi.org/10.1016/j.enconman.2016.02.037>
- Zhang, D.Q., Tan, S.K., Gersberg, R.M.: Municipal solid waste management in China: status, problems and challenges. *J. Environ. Manage.* **91**(8), 1623–1633 (2010). <https://doi.org/10.1016/j.jenvman.2010.03.012>
- Nisar, J., Ali, G., Shah, A., Iqbal, M., Khan, R.A., Sirajuddin, Anwar, F., Ullah, R., Akhter, M.S.: Fuel production from waste polystyrene via pyrolysis: kinetics and products distribution. *Waste Manage.* **88**, 236–247 (2019). <https://doi.org/10.1016/j.wasman.2019.03.035>
- Mishra, R.K., Iyer, J.S., Mohanty, K.: Conversion of waste biomass and waste nitrile gloves into renewable fuel. *Waste Manage.* **89**, 397–407 (2019). <https://doi.org/10.1016/j.wasman.2019.04.032>
- Veses, A., Sanahuja-Parejo, O., Callen, M.S., Murillo, R., Garcia, T.: A combined two-stage process of pyrolysis and catalytic cracking of municipal solid waste for the production of syngas and solid refuse-derived fuels. *Waste Manage.* **101**, 171–179 (2020). <https://doi.org/10.1016/j.wasman.2019.10.009>
- Blazquez, F.C., Gonzalez, A.G., Sanchez, C.S., Rodriguez, V.D., Salcedo, F.C.: Waste valorization as an example of circular economy in extremadura (Spain). *J. Clean. Prod.* **181**, 136–144 (2018). <https://doi.org/10.1016/j.jclepro.2018.01.228>
- Hidalgo, D., Martin-Marroquin, J.M., Corona, F.: A multi-waste management concept as a basis towards a circular economy model. *Renew. Sust. Energy Rev.* **11**, 481–489 (2019). <https://doi.org/10.1016/j.rser.2019.05.048>
- Antoniou, N., Monlau, F., Sambusiti, C., Ficara, E., Barakat, A., Zabaniotou, A.: Contribution to circular economy options of mixed agricultural wastes management: coupling anaerobic digestion with gasification for enhanced energy and material

- recovery. *J. Clean. Prod.* **209**, 505–514 (2019). <https://doi.org/10.1016/j.jclepro.2018.10.055>
12. Paraschiv, M., Kuncser, R., Tazerout, M., Prisecaru, T.: New energy value chain through pyrolysis of hospital plastic waste. *Appl. Therm. Eng.* **87**, 424–433 (2015). <https://doi.org/10.1016/j.applthermaleng.2015.04.070>
 13. Chen, L., Wang, S.Z., Meng, H.Y., Wu, Z.Q., Zhao, J.: Synergistic effect on thermal behavior and char morphology analysis during co-pyrolysis of paulownia wood blended with different plastics waste. *Appl. Therm. Eng.* **111**, 834–846 (2017). <https://doi.org/10.1016/j.applthermaleng.2016.09.155>
 14. Navarro, M.V., Lopez, J.M., Veses, A., Callen, M.S., Garcia, T.: Kinetic study for the co-pyrolysis of lignocellulosic biomass and plastics using the distributed activation energy model. *Energy* **165**, 731–742 (2018). <https://doi.org/10.1016/j.energy.2018.09.133>
 15. Chen, R.Y., Xu, X.K., Zhang, Y., Lo, S.M., Lu, S.X.: Kinetic study on pyrolysis of waste phenolic fibre-reinforced plastic. *Appl. Therm. Eng.* **136**, 484–491 (2018). <https://doi.org/10.1016/j.applthermaleng.2018.03.045>
 16. Singh, R.K., Ruj, B., Sadhukhan, A.K., Gupta, P.: Impact of fast and slow pyrolysis on the degradation of mixed plastic waste: product yield analysis and their characterization. *J. Energy Inst.* **92**(6), 1647–1657 (2019). <https://doi.org/10.1016/j.joei.2019.01.009>
 17. Ippolito, N.M., Cafiero, L., Tuffi, R., Cipriotti, S.V.: Characterization of the residue of a commingled post-consumer plastic waste treatment plant: a thermal, spectroscopic and pyrolysis kinetic study. *J. Therm. Anal. Calorim* **138**(5), 3323–3333 (2019). <https://doi.org/10.1007/s10973-019-09003-z>
 18. Chhabra, V., Bhattachary, S., Shastri, Y.: Pyrolysis of mixed municipal solid waste: characterisation, interaction effect and kinetic modelling using the thermogravimetric approach. *Waste Manage.* **90**, 152–167 (2019). <https://doi.org/10.1016/j.wasman.2019.03.048>
 19. Teng, S.Y., Loy, A.C.M., Leong, W.D., How, B.S., Chin, B.L.F., Masa, V.: Catalytic thermal degradation of *Chlorella vulgaris*: evolving deep neural networks for optimization. *Bioresour. Technol.* **292**, 121971 (2019). <https://doi.org/10.1016/j.biortech.2019.121971>
 20. Quesada, L., Perez, A., Godoy, V., Peula, F.J., Calero, M., Blázquez, G.: Optimization of the pyrolysis process of a plastic waste to obtain a liquid fuel using different mathematical models. *Energy. Convers. Manage.* **188**, 19–26 (2019). <https://doi.org/10.1016/j.enconman.2019.03.054>
 21. Sadeghizadeh, A., Ebrahimi, F., Heydari, M., Tahmasebikohyani, M., Ebrahimi, F., Sadeghizadeh, A.: Adsorptive removal of Pb (II) by means of hydroxyapatite/chitosan nanocomposite hybrid nano-adsorbent: ANFIS modeling and experimental study. *J. Environ. Manage.* **232**, 342–353 (2019). <https://doi.org/10.1016/j.jenvman.2018.11.047>
 22. Ronda, A., Martín-Lara, M.A., Almendros, A.I., Pérez, A., Blázquez, G.: Comparison of two models for the biosorption of Pb(II) using untreated and chemically treated olive stone: experimental design methodology and adaptive neural fuzzy inference system (ANFIS). *J. Taiwan Inst. Chem. Eng.* **54**, 45–56 (2015). <https://doi.org/10.1016/j.jtice.2015.03.004>
 23. Calero, M., Iañez-Rodríguez, I., Perez, A., Martín-Lara, M.A., Blázquez, G.: Neural fuzzy modelization of copper removal from water by biosorption in fixed-bed columns using olive stone and pinion shell. *Bioresour. Technol.* **252**, 100–109 (2018). <https://doi.org/10.1016/j.biortech.2017.12.074>
 24. Iañez-Rodríguez, I., Martín-Lara, M.A., Blázquez, G., Pérez, A., Calero, M.: Effect of torrefaction conditions on greenhouse crop residue: optimization of conditions to upgrade solid characteristics. *Bioresour. Technol.* **244**, 741–749 (2017). <https://doi.org/10.1016/j.biortech.2017.08.031>
 25. Javed, M.S., Song, A.T., Ma, T.: Techno-economic assessment of a stand-alone hybrid solar-wind-battery system for a remote island using genetic algorithm. *Energy* **176**, 704–717 (2019). <https://doi.org/10.1016/j.energy.2019.03.131>
 26. Tuchler, S., Chen, Z.H., Copeland, C.D.: Multipoint shape optimisation of an automotive radial compressor using a coupled computational fluid dynamics and genetic algorithm approach. *Energy* **165**, 543–561 (2018). <https://doi.org/10.1016/j.energy.2018.09.076>
 27. Ascione, F., Bianco, N., Mauro, G.M., Napolitano, D.F.: Building envelope design: multi-objective optimization to minimize energy consumption, global cost and thermal discomfort. Application to different Italian climatic zones. *Energy* **174**, 359–374 (2019). <https://doi.org/10.1016/j.energy.2019.02.182>
 28. Rezaie, A., Tsatsaronis, G., Hellwig, U.: Thermal design and optimization of a heat recovery steam generator in a combined-cycle power plant by applying a genetic algorithm. *Energy* **168**, 346–357 (2019). <https://doi.org/10.1016/j.energy.2018.11.047>
 29. Akgün, H., Yapıcı, E., Günkaya, Z., Özkan, A., Banar, M.: Utilization of liquid product through pyrolysis of LDPE and C/LDPE as commercial wax. *Environ. Sci. Pollut. Res.* (2021). <https://doi.org/10.1007/s11356-021-13999-z>
 30. Chen, R.Y., Xu, X.K., Lu, S.X., Zhang, Y., Lo, S.M.: Pyrolysis study of waste phenolic fibre-reinforced plastic by thermogravimetry/Fourier transform infrared/mass spectrometry analysis. *Energy Convers. Manage.* **165**, 555–566 (2018). <https://doi.org/10.1016/j.enconman.2018.03.092>
 31. Aboulkas, A., El Harfi, K., El Bouadili, A.: Thermal degradation behaviors of polyethylene and polypropylene. Part I: pyrolysis kinetics and mechanisms. *Energy Convers. Manage.* **51**(7), 1363–1369 (2010). <https://doi.org/10.1016/j.enconman.2009.12.017>
 32. Mumbach, G.D., Alves, J.L.F., Da Silva, J.C.G., De Sena, R.F., Marangoni, C., Machado, R.A.F., Bolzan, A.: Thermal investigation of plastic solid waste pyrolysis via the deconvolution technique using the asymmetric double sigmoidal function: determination of the kinetic triplet, thermodynamic parameters, thermal lifetime and pyrolytic oil composition for clean energy recovery. *Energy Convers. Manage.* **200**, 112031 (2019). <https://doi.org/10.1016/j.enconman.2019.112031>
 33. Sousa, V., Meireles, I., Oliveira, V., Dias-Ferreira, C.: Prediction performance of separate collection of packaging waste yields using genetic algorithm optimized support vector machines. *Waste Biomass Valorization* **10**(12), 3603–3612 (2019). <https://doi.org/10.1007/s12649-019-00656-3>
 34. Michailos, S., Parker, D., Webb, C.: Design, sustainability analysis and multiobjective optimisation of ethanol production via syngas fermentation. *Waste Biomass Valorization* **10**(4), 865–876 (2019). <https://doi.org/10.1007/s12649-017-0151-3>
 35. Barik, D., Murugan, S.: An artificial neural network and genetic algorithm optimized model for biogas production from co-digestion of seed cake of Karanja and cattle dung. *Waste Biomass Valorization* **6**(6), 1015–1027 (2015). <https://doi.org/10.1007/s12649-015-9392-1>
 36. Perez-Gallardo, J.R., Azzaro-Pantel, C., Astier, S.: A multi-objective framework for assessment of recycling strategies for photovoltaic modules based on life cycle assessment. *Waste Biomass Valorization* **9**(1), 147–159 (2018). <https://doi.org/10.1007/s12649-017-9878-0>
 37. Niu, B., Jia, M., Xu, G.F., Chang, Y.C., Xie, M.Z.: Efficient approach for the optimization of skeletal chemical mechanisms with multiobjective genetic algorithm. *Energy Fuel* **32**(6), 7086–7102 (2018). <https://doi.org/10.1021/acs.energyfuels.8b00356>

38. Das, P., Tiwari, P.: Thermal degradation kinetics of plastics and model selection. *Thermochim. Acta* **654**, 191–202 (2017). <https://doi.org/10.1016/j.tca.2017.06.001>
39. Das, P., Tiwari, P.: Thermal degradation study of waste polyethylene terephthalate (PET) under inert and oxidative environments. *Thermochim. Acta* **679**, 178340 (2019). <https://doi.org/10.1016/j.tca.2019.178340>
40. Pan, R.M., Duque, J.V.F., Debenest, G.: Investigating waste plastic pyrolysis kinetic parameters by genetic algorithm coupled with thermogravimetric analysis. *Waste Biomass Valorization* **12**, 2623–2637 (2021). <https://doi.org/10.1007/s12649-020-01181-4>
41. Pan, R.M., Duque, J.V.F., Martins, M.F., Debenest, G.: Application of a neural fuzzy model combined with simulated annealing algorithm to predict optimal conditions for polyethylene waste non-isothermal pyrolysis. *Heliyon* **6**(11), e05598 (2020). <https://doi.org/10.1016/j.heliyon.2020.e05598>
42. Duque, J.V.F., Martins, M.F., Debenest, G., Orlando, M.T.D.: The influence of the recycling stress history on LDPE waste pyrolysis. *Polym. Test.* **86**, 106460 (2020). <https://doi.org/10.1016/j.polymertesting.2020.106460>
43. Majid, M., Chin, B.L.F., Jawad, Z.A., Chai, Y.H., Lam, M.K., Yusup, S., Cheah, K.W.: Particle swarm optimization and global sensitivity analysis for catalytic co-pyrolysis of *Chlorella vulgaris* and plastic waste mixtures. *Bioresour. Technol.* **329**, 124874 (2021). <https://doi.org/10.1016/j.biortech.2021.124874>
44. Pan, R.M., Martins, M.F., Debenest, G.: Pyrolysis of waste polyethylene in a semi-batch reactor to produce liquid fuel: optimization of operating conditions. *Energy Convers. Manag.* **237**, 114114 (2021). <https://doi.org/10.1016/j.enconman.2021.114114>
45. Bong, J.T., Loy, A.C.M., Chin, B.L.F., Lam, M.K., Tang, D.K.H., Lim, H.Y., Chai, Y.H., Yusup, S.: Artificial neural network approach for co-pyrolysis of *Chlorella vulgaris* and peanut shell binary mixtures using microalgae ash catalyst. *Energy* **207**, 118289 (2020). <https://doi.org/10.1016/j.energy.2020.118289>
46. Liew, J.X., Loy, A.C.M., Chin, B.L.F., AlNouss, A., Shahbaz, M., Al-Ansari, T., Govindan, R., Chai, Y.H.: Synergistic effects of catalytic co-pyrolysis of corn cob and HDPE waste mixtures using weight average global process model. *Renew. Energy* **170**, 948–963 (2021). <https://doi.org/10.1016/j.renene.2021.02.053>
47. Singh, R.K., Ruj, B., Sadhukhan, A.K., Gupta, P.: Thermal degradation of waste plastics under non-sweeping atmosphere: part 1: effect of temperature, product optimization, and degradation mechanism. *J. Environ. Manage.* **239**, 395–406 (2019). <https://doi.org/10.1016/j.jenvman.2019.03.067>
48. Wang, X.B., Liang, Q.M., Wang, J.N., Bai, S.J., Mikulčić, H., Vujanović, M., Tan, H.Z.: Synergistic effect of biomass and polyurethane waste co-pyrolysis on soot formation at high temperatures. *J. Environ. Manage.* **239**, 306–315 (2019). <https://doi.org/10.1016/j.jenvman.2019.03.073>
49. Zhang, J.Z., Chen, T.J., Wu, J.L., Wu, J.H.: A novel Gaussian-DAEM-reaction model for the pyrolysis of cellulose, hemicellulose and lignin. *RSC Adv.* **4**, 17513–17520 (2014). <https://doi.org/10.1039/C4RA01445F>

Publisher's Note Springer Nature remains neutral with regard to jurisdictional claims in published maps and institutional affiliations.

Authors and Affiliations

Ruming Pan¹ · João Vitor Ferreira Duque^{1,2,3} · Gérald Debenest¹

¹ Institut de Mécanique des Fluides de Toulouse (IMFT), CNRS-INPT-UPS, Université de Toulouse, 31400 Toulouse, France

² Federal Institute of Education, Science and Technology of Espírito Santo, Serra 29173-087, Brazil

³ Laboratory of Combustion and Combustible Matter (LCC), PPGEM, Federal University of Espírito Santo, Vitória 29075-910, Brazil